International Forum on Aeroelasticity and Structural Dynamics
IFASD 2024
17-21 June 2024, The Hague, The Netherlands

# AEROSERVOELASTIC ANALYSIS AND LOAD ALLEVIATION CONTROL FOR VERY FLEXIBLE AIRCRAFT: TU-FLEX STUDY

**Guilherme C. Barbosa**[1], **Álvaro A. G. Quesada**[1], **Pedro J. González**[1], **Gerrit Stavorinus**[1], **Flávio J. Silvestre**[1]

[1]Technical University of Berlin
Marchstraße 12, 10587 Berlin, Germany
g.chaves.barbosa@tu-berlin.de
garcia.quesada@campus.tu-berlin.de
p.gonzalez.ramirez@tu-berlin.de
gerrit.s.stavorinus@campus.tu-berlin.de
flavio.silvestre@tu-berlin.de

**Keywords:** High Aspect Ratio, Aeroservoelasticity, Load Alleviation, Time-delay, Servo Dynamics

**Abstract:** This paper performs an aeroservoelastic analysis and load alleviation control design for very flexible aircraft. This research aims to address the challenges posed by the increasing flexibility of modern aircraft and develop control systems to alleviate loads on the aircraft. The study takes into account the dynamic interaction between the actuator and time-delay dynamics and the elastic modes of the aircraft in order to improve the controller performance and stability. Utilizing a control law design procedure based on a unified formulation of the flexible aircraft, the study achieved significant attenuation of both structural loads and rigid-body motions. This finding indicates the potential for enhanced flight handling qualities and improved system stability.

## 1 INTRODUCTION

Recent years have seen a growing need in the aeronautical industry to develop solutions that improve aircraft aerodynamic efficiency, reducing fuel consumption and carbon emissions. High Aspect Ratio (HAR) wings have emerged as a promising approach for achieving these goals by increasing wing span and using lighter materials to reduce overall aircraft weight. However, the advantages of more slender and lighter weight wings come with increased deformation and lower structural frequencies, making the traditional rigid-body approximation invalid for analyzing flight dynamics of such aircraft due to the coupling between flight dynamics and aeroelastic modes [1].

Modern aerospace vehicles heavily rely on active control systems, as noted in the literature [2]. For highly flexible aircraft like those with HAR wings, control system design demands more intricate models and techniques compared to their less flexible counterparts. This increased complexity arises from the inherent coupling between the aircraft's structure, control system, and actuators, a phenomenon known in the field as aeroservoelasticity [3]. Consequently, achieving desired aeroelastic characteristics necessitates accurate system modeling that incorporates these additional dynamics [4, 5].

Livne [6] has compiled a thorough overview of the current advancements and future requirements in the field of active flutter suppression (AFS). Significant research in this area includes

work by Burnett and colleagues at Lockheed Martin Corporation and the Air Force Research Laboratory [7], the FLEXOP European project [8–10], and studies by David K. Schmidt and his team [11, 12]. These investigations have introduced and tested various integrated flight and aeroelastic control methods, showing considerable enhancements in flying qualities and broadening the flight envelope.

The complex interaction between flight dynamics and aeroelastic modes in highly flexible aircraft, particularly those with HAR, poses a significant challenge for accurate modeling. The lack of experimental data on coupled flight and structural dynamics for highly flexible aircraft also hinders the improvement of modeling techniques.

Bridging the data gap is a key objective of the TU-Flex flight demonstrator, which is a collaborative project between TU-Berlin and DLR [13]. This platform utilizes a HAR wing configuration, emulating a transport aircraft. This configuration facilitates the collection of integrated flight and structural dynamics data for research purposes. Its modular design allows for easy wing exchange, facilitating tests with increasingly flexible wing sets. The initial version offers two wing options: a Flexible Wing allowing tip deflections up to 10% of the wing semi-span, and a very-flexible wing permitting deflections of up to 20%. See Fig. 1 for an illustration of the TU-Flex demonstrator.

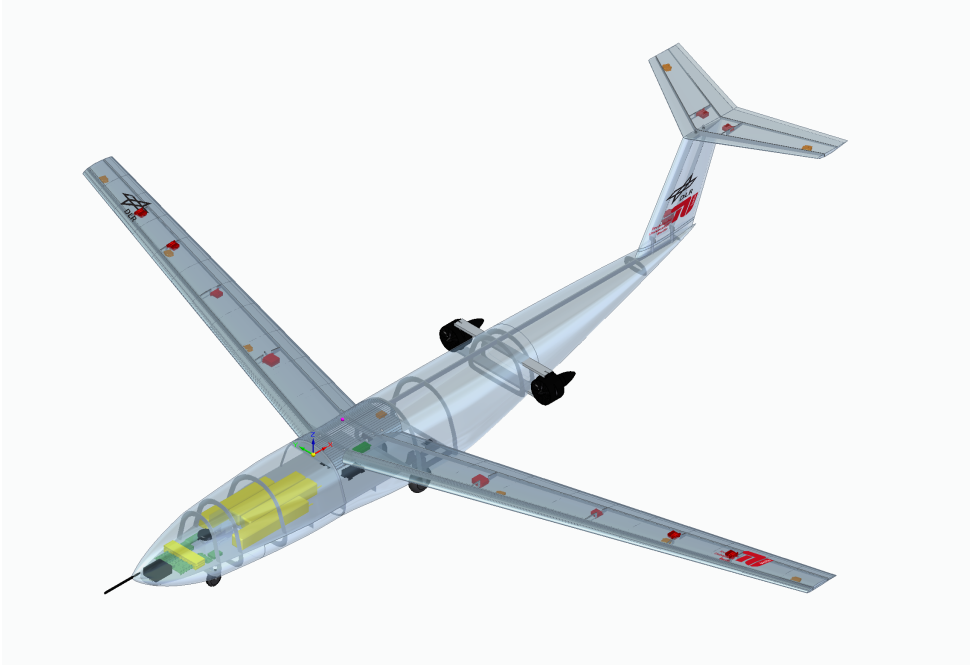

Figure 1: TU-Flex and systems

The TU-Flex platform goes beyond data acquisition and model validation. It is a valuable tool for exploring the effects of flexibility on aircraft controller design, which is crucial for addressing the challenges of controlling highly flexible aircraft, including implementing active load alleviation methods.

This paper will apply a load alleviation control to the TU-Flex model based on the method proposed by Silvestre et al. [14]. This method uses modal amplitudes derivative ($\dot{\eta}$) feedback, reducing the loads at the fuselage. An important aspect of this study is to analyze the impact of actuator dynamics and time-delays on the performance and stability of the control system. As shown by Sereni et al. [15], even small time-delays (0.02 seconds) can significantly affect

stability or lead to instability, highlighting the importance of incorporating these dynamics from the outset of the control design process.

The remainder of the paper is structured as follows. Section 2 details the TU-Flex platform and its systems, along with the numerical models employed. Section 3 focuses on the control design process, addressing the interaction of rigid-body control with flexible modes, the impact of actuators and time-delay dynamics on performance and stability, and culminating in simulation results that validate the effectiveness of the load alleviation control. Section 4 concludes the paper by summarizing the key findings.

## 2 TU-FLEX PLATFORM

Developing next-generation, eco-friendly aircraft faces a significant challenge due to the absence of cost-effective flying platforms with flexible wings similar to those of commercial airliners [16, 17]. These platforms are essential for collecting data on how an aircraft's structure interacts with its flight dynamics. To bridge this gap, the Chair of Flight Mechanics, Flight Control and Aeroelasticity at TU Berlin partnered with the German Aerospace Center's Institute of Aeroelasticity to initiate the development of TU-Flex.

TU-Flex, a flying testbed designed to reflect the configuration of future commercial and transport aircraft, serves as a platform for analyzing how increased wing flexibility affects flight dynamics and control systems. This understanding will contribute to the design of more efficient and environmentally friendly airplanes. The conceptual design drew inspiration from existing flying demonstrators such as T-2, S-2, IEP, PTERA, P-GMATT, and AlbatrossONE [18–22]. Furthermore, established flying aeroelastic testbeds like X-HALE, FLEXOP, mAEwing, and Huginn [9, 11, 23–25] were also considered during the conceptual design process. By studying these aircraft designs in detail, the research team behind TU-Flex was able to determine suitable flight envelope instrumentation requirements, as well as key design considerations. TU-Flex was designed to be flown as a remotely piloted airplane in line of sight in a controlled unpopulated area.

TU-Flex features both flexible and very-flexible wings, designed to comply with the designated operational and facility restrictions. To ensure maximum wing tip displacement during normal 1g cruise flight, structural optimization was carried out while considering geometric constraints on the wingtip twist angle. The design load cases were set at +6g and -3g for the flexible wing to represent the maximum expected forces. However, taking into account the increased flexibility of the VFA wings, lower limits of +4g and -2g were chosen for these load cases. These selections were carefully made based on insights gained from previous experiments with similar demonstrators in consideration of the anticipated flight envelope [23].

One of TU-Flex's key strengths lies in its modular design. This approach integrates the propulsion system, computers, rigid body, and structural dynamics measurement system into the fuselage. This modularity allows for the easy exchange of wings while keeping the core systems that power, control, and gather crucial aero/rigid/structural data consistent. This design philosophy enables efficient testing of various wing configurations using the same platform. For a more detailed description of the demonstrator, its requirements, design limitations, and performance capabilities, please refer to the description of González et al. [13].

### 2.1 Numerical Model

The initial geometric model of TU-Flex, incorporating preliminary design wings, was developed using OpenVSP [26]. Subsequently, the fuselage and tail assembly were further imported in Altair HyperMesh [27] to generate a high-fidelity Finite Element (FE) model for detailed structural analysis [17]. The structural FE models for both the Flexible Wing (FW) and Very Flexible Wing (VFW) sets of TU-Flex were generated using the in-house software ModGen [28, 29] at the DLR Institute of Aeroelasticity [16, 17]. In Tab. 1 and 2 the natural frequencies of the first eighth modes considered on this study for the TU-Flex flexible and very flexible configuration are depicted.

With the purpose of aeroelastic analysis and control application, a low-order aircraft model of TU-Flex (flexible and very flexible configurations) from the FE MSC Nastran model has been generated using ModSiG-FMRA [30]. The Modeling and Simulation Group Toolbox created by the Chair of Flight Mechanics, Flight Control and Aeroelasticity of TU Berlin is a low-order framework for modeling, analyzing, and simulating very-flexible/flexible wings and aircraft (ModSiG-FMRA). It uses mean axes formulation, modal superposition for structural dynamics, therefore considered linear, nonlinear flight mechanics, and quasi-steady or unsteady strip theory for incremental aerodynamics due to elastic deformations. The aerodynamic formulation permits to incorporate stall effects and/or follower forces. In this paper unsteady aerodynamics considering stall effects has been selected for the TU-Flex aircraft models (flexible and very flexible configuration).

The vector of state variables for the full-order nonlinear model is given by

$$\mathbf{x} = [V, \theta, H, \alpha, q, \beta, r, \phi, p, \Psi, x_e, y_e, \eta, \dot{\eta}, \lambda_\mathbf{1}, \lambda_\mathbf{2}] \tag{1}$$

where $V$ is the velocity; $\theta$ is the pitch Euler angle; $H$ is the altitude; $\alpha$ is the angle of attack; $q$ is the pitch rate; $\beta$ is the sideslip angle; $r$ is the yaw angular velocity; $\phi$ is the roll Euler angle; $p$ is the roll angular velocity; $\Psi$ is the yaw Euler Angle; $x_e$ is the x trajectory coordinate

Table 1: TU-Flex aircraft FE model modal frequencies with flexible wing set.

| # | Mode type | Frequency (Hz) |
|---|---|---|
| 1 | Wing $1^{st}$ Symmetric Bending Out-of-Plane | 4.73 |
| 2 | Wing $1^{st}$ Asymmetric Bending Out-of-Plane | 7.89 |
| 3 | Wing $2^{nd}$ Asymmetric Bending Out-of-Plane + Vertical Empennage $1^{st}$ Bending Out-of-Plane | 12.87 |
| 4 | Wing $2^{nd}$ Symmetric Bending Out-of-Plane + Horizontal Empennage $1^{st}$ Symmetric Bending Out-of-Plane | 17.29 |
| 5 | Wing $2^{nd}$ Asymmetric Bending Out-of-Plane + Vertical Empennage $1^{st}$ Torsion | 19.18 |
| 6 | Horizontal Empennage $1^{st}$ Asymmetric Bending Out-of-Plane + Vertical Empennage $1^{st}$ Torsion | 19.80 |
| 7 | Fuselage $1^{st}$ Bending Out-of-Plane + Horizontal Empennage $1^{st}$ Symmetric Bending Out-of-Plane | 21.83 |
| 8 | Vertical Empennage $1^{st}$ Torsion + Wing $1^{st}$ Asymmetric Bending In-Plane | 24.54 |

Table 2: TU-Flex aircraft FE model modal frequencies with very-flexible wing set.

| # | Mode type | Frequency (Hz) |
|---|---|---|
| 1 | Wing $1^{st}$ Symmetric Bending Out-of-Plane | 1.69 |
| 2 | Wing $2^{nd}$ Asymmetric Bending Out-of-Plane | 4.59 |
| 3 | Wing $2^{nd}$ Asymmetric Bending Out-of-Plane + Vertical Empennage $1^{st}$ Bending Out-of-Plane | 9.40 |
| 4 | Wing $1^{st}$ Symmetric Bending In-Plane + Wing $2^{nd}$ Symmetric Bending Out-of-Plane | 10.46 |
| 5 | Wing $2^{nd}$ Symmetric Bending Out-of-Plane | 10.55 |
| 6 | Wing $2^{nd}$ Asymmetric Bending Out-of-Plane + Wing $1^{st}$ Asymmetric Bending In-Plane + Vertical Empennage $1^{st}$ Torsion | 12.64 |
| 7 | Wing $2^{nd}$ Asymmetric Bending Out-of-Plane + Vertical Empennage $1^{st}$ Bending Out-of-Plane + Vertical Empennage $1^{st}$ Torsion | 16.31 |
| 8 | Horizontal Empennage $1^{st}$ Symmetric Bending Out-of-Plane + Fuselage $1^{st}$ Bending Out-of-Plane | 21.77 |

in the Earth Reference Frame (ERF, considered as the Inertial Reference Frame); $y_e$ is the y trajectory coordinate in the ERF; $\eta$ and $\dot{\eta}$ are the elastic modal amplitudes and their derivatives (each vector consists of as many positions as number of modes considered); $\lambda_\mathbf{1}$ and $\lambda_\mathbf{2}$ are the lag states due to airfoil arbitrary motion (each vector consists of as many positions as number of aerodynamic strips). The input vector is

$$\mathbf{u} = [m, \delta_e, \delta_{ai,r}, \delta_{ai,l}, \delta_{am,r}, \delta_{am,l}, \delta_{ae,r}, \delta_{ae,l}, \delta_{f,r}, \delta_{f,l}, \delta_r, \delta_T, w_x, w_y, w_z] \tag{2}$$

where $m$ is the aircraft mass; $\delta_e$ is the elevator deflection; $\delta_{ai,r}$ and $\delta_{ai,l}$ are the left and right inner aileron deflections; $\delta_{am,r}$ and $\delta_{am,l}$ are the left and right mid aileron deflections; $\delta_{ae,r}$ and $\delta_{ae,l}$ are the left and right external aileron deflections; $\delta_{f,r}$ and $\delta_{f,l}$ are the left and right flap deflections; $\delta_r$ is the rudder deflection; $\delta_T$ is the throttle per engine; and $w_x$, $w_y$ and $w_z$ are the wind components in ERF. The computed outputs can be defined according to the needs of the user. For this study the output variables are

$$\mathbf{y} = [V, \theta, H, \alpha, q, \beta, r, \phi, p, \Psi, x_e, y_e, \eta, \dot{\eta}, \epsilon_{root,r}, \epsilon_{root,l}, Tz_r, Tz_l] \tag{3}$$

where $\epsilon_{root}$ represents the measurement of the strain gauges on the root (vertical load), and $Tz$ represents the wing tip vertical displacement. The remaining outputs correspond to the states defined in Eq. (1), excluding the lag states.

Employing linearization through the theory of small perturbations, the state-space matrices of the system are derived, where $\mathbf{A} \in R^{128\times128}$ is the state matrix, $\mathbf{B} \in R^{128\times15}$ is the control matrix, $\mathbf{C} \in R^{32\times128}$ is the output matrix and $\mathbf{D} \in R^{32\times15}$ is the direct-feed matrix.

### 2.2 System Description

The TU-Flex aircraft employs a distributed electrical and electronic systems architecture. This architecture is divided into four distinct categories based on their primary functions: propulsion

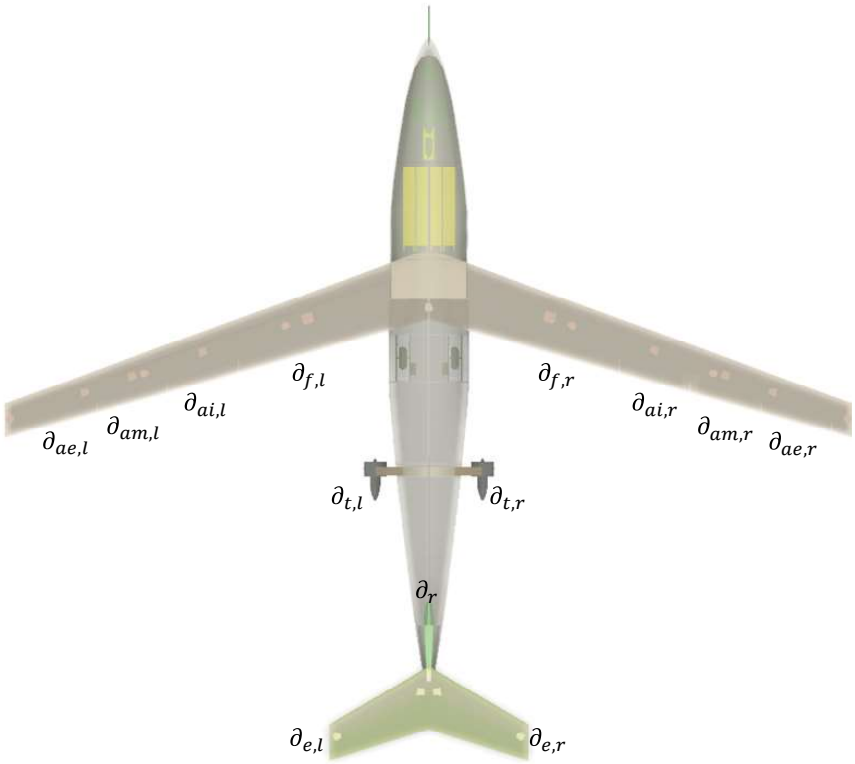


Figure 2: Actuators position and nomenclature.

system; Flight Control System (FCS); Data Acquisition and Transmission System (DATS); and electrical power system. The electrical circuitry for these functional categories is strategically distributed throughout the aircraft. Interconnectivity between these systems is achieved through a network of cables routed within the wings, fuselage, and tail assembly.

The TU-Flex aircraft utilizes a twin electric motor configuration for its propulsion system. These motors are specifically identified as Schübeler DS-51-DIA HST models. To characterize the performance of the propulsive group across the entire operational airspeed range, wind tunnel testing was conducted [31]. The analysis presented in this paper leverages a simplified transfer function derived from the wind tunnel test results.

The TU-Flex aircraft utilizes a differentiated servo selection strategy for its control surface actuation system. This approach balances the trade-off between actuation speed and torque requirements for different control surfaces. Elevators and Ailerons (Inner, Middle, and Outer) employ Volz DA 15-N-ISS servos, prioritizing faster actuation for precise maneuver control. Flaps and rudder utilize the Volz DA 20 servos, which offer higher torque capabilities to handle larger aerodynamic loads. A visual representation of the actuator locations and designations can be found in Fig. 2. In the figure, ”$\delta$” denotes the actuator symbol, with subscripts indicating the specific control surface (”a” for aileron, ”f” for flap, ”T” for throttle, ”r” for rudder, and ”e” for elevator), side position (”r” for right side and ”l” for left side), and wing position for the ailerons (”e” for external, ”m” for mid, and ”i” for internal).

The DATS within TU-Flex serves as the interface between various onboard sensors and the FCS. Its primary functions include: acquiring critical flight data from various sensors, processing the acquired data, and transmitting the processed data to the FCS for real-time control. The DATS hardware consists of ten Inertial Measurement Units (IMUs), one GNSS/INS unit (Global Navigation Satellite System/Inertial Navigation System), one five-hole Pitot probe for airspeed

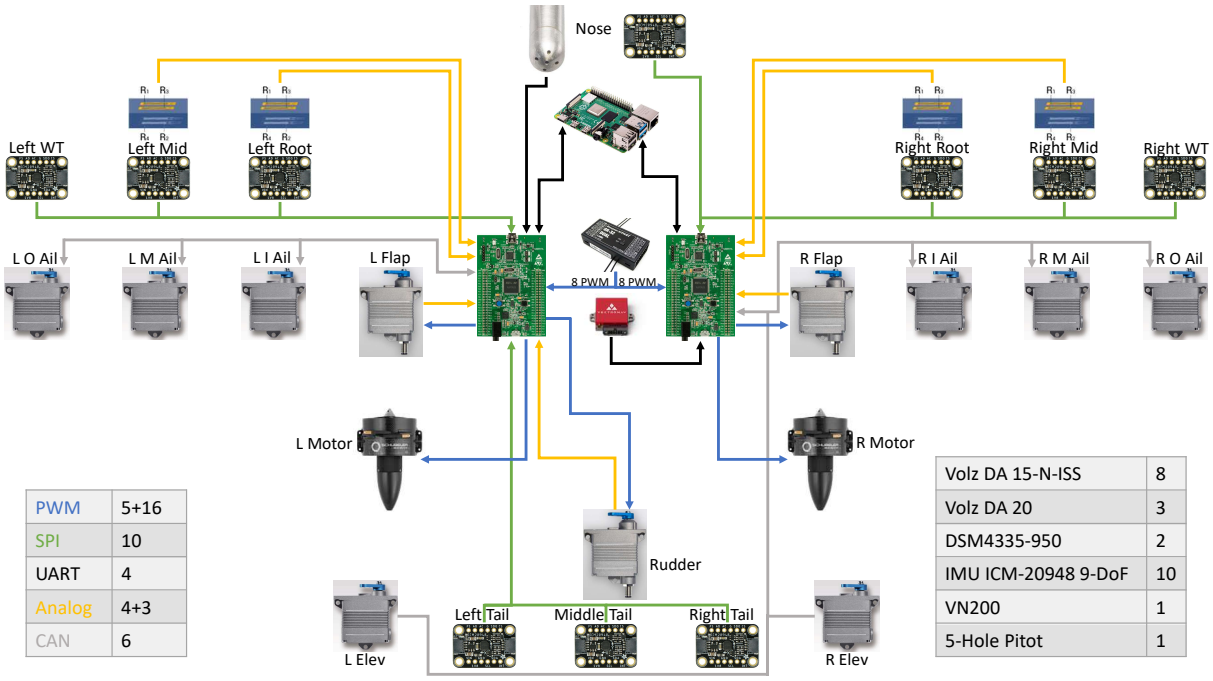


Figure 3: TU-Flex system schematic.

and angle of attack measurements, and two data acquisition boards responsible for interfacing with the sensors and processing the collected data.

The FCS acts as the brain of the TU-Flex, utilizing the processed flight data received from the DATS to control the aircraft's actuators and motors. The FCS functionality can be categorized based on the selected operational mode:

- Direct Pilot Control: In this mode, pilot commands are directly transmitted to the actuators, enabling manual flight control.
- Stability Augmentation System (SAS): This mode utilizes the FCS to implement an automated control loop that enhances the aircraft's flight characteristics and stability. This

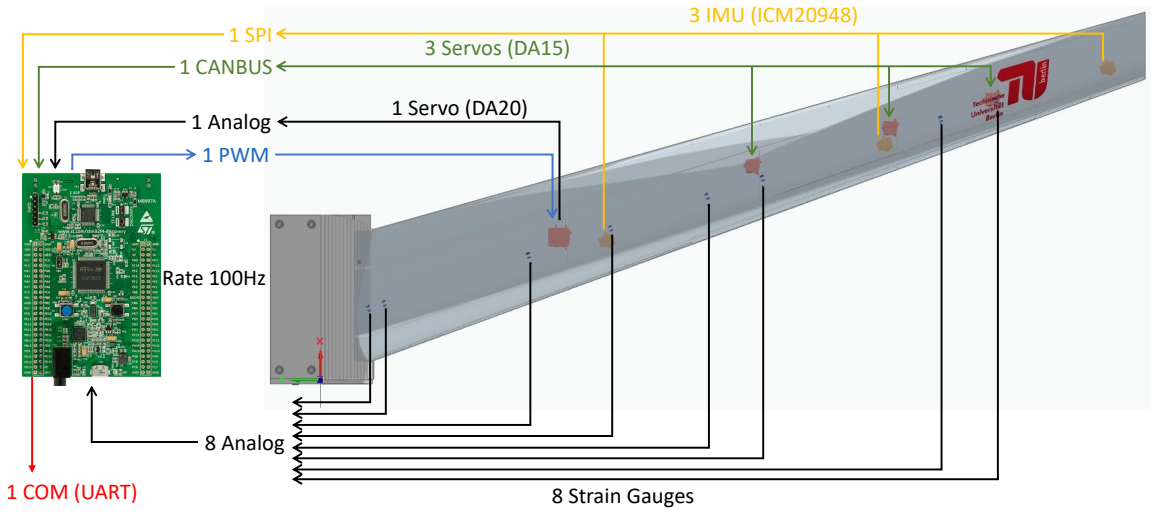


Figure 4: TU-Flex wing system schematic for the wind tunnel test campaign.

improves handling qualities and reduces pilot workload.
- Pre-programmed Maneuvers: The FCS can execute pre-programmed flight maneuvers for specific test scenarios or demonstration purposes.

A detailed communication schematic between these systems is illustrated in Fig. 3.

Employing a phased construction and testing approach, the TU-Flex project initially focused on the right wing. This wing was constructed, instrumented with sensors, and subsequently evaluated through a wind tunnel testing campaign [32]. A simplified schematic depicting the wing test setup is presented in Fig. 4. Note that for the wing only one STM32 board is actuating as DATS and FCS at the same time.

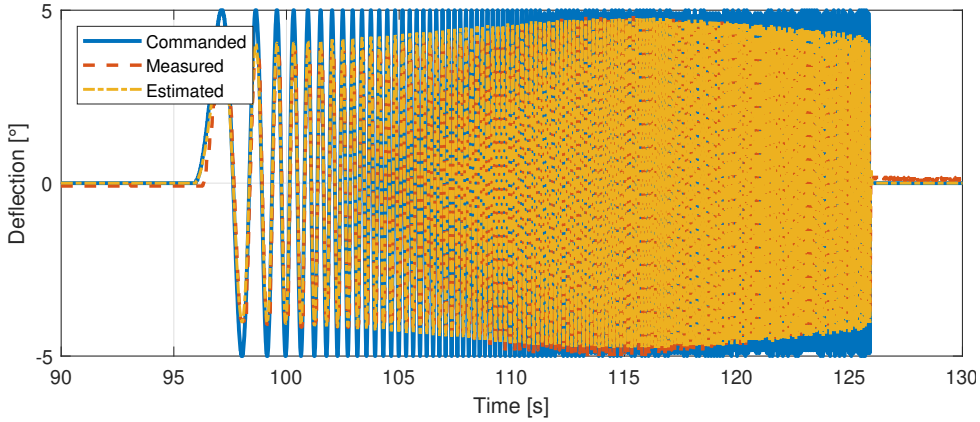


Figure 5: A sweep signal with a 5-degree amplitude and a frequency linearly varying from 0 to 10 Hz applied to the mid aileron.

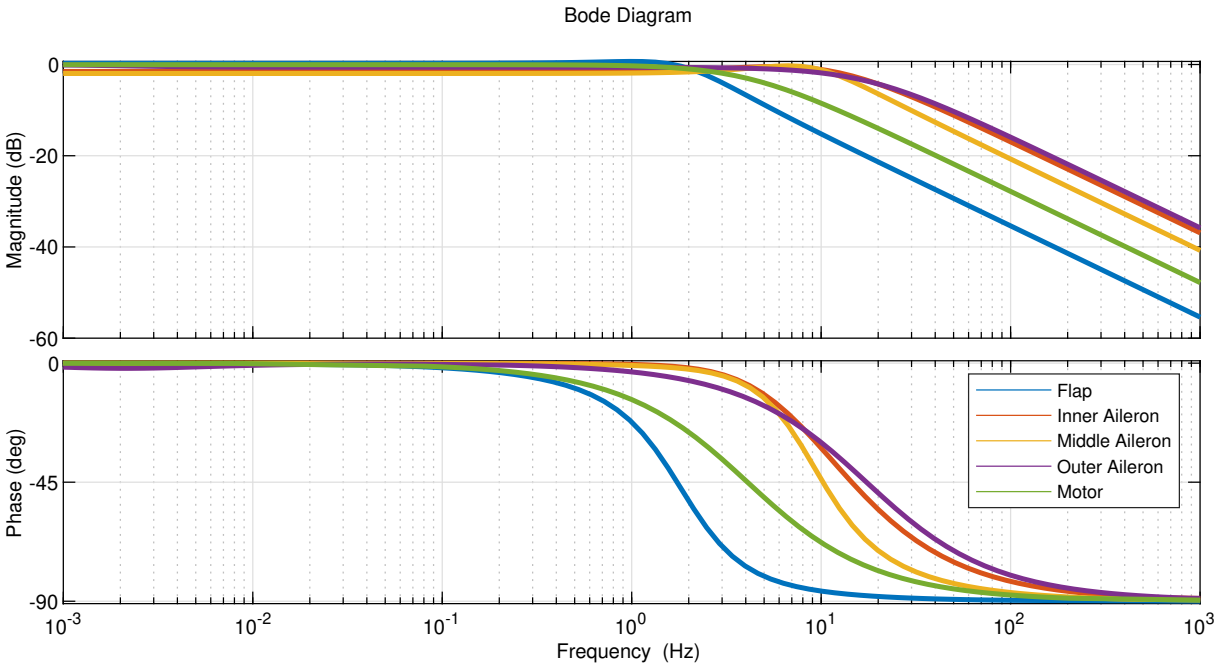


Figure 6: Bode plot of the estimated transfer functions representing the actuator dynamics.

The wind tunnel tests provided valuable data for estimating the dynamic characteristics of the ailerons and flap actuators. During a test conducted at 30 m/s, sweep signals were applied to the actuators, and the corresponding position signals were recorded, as shown in Fig. 5 a

sweep signal with 5 deg amplitude and frequency varying linearly from 0 to 10 Hz. These measurements were then utilized to estimate the transfer functions of the actuator dynamics, which are shown in Fig. 6 as Bode plots. Interestingly, the results revealed that even though the same servo model was used for all ailerons, slight variations in control surface size and construction processes resulted in measurable differences in their estimated dynamics. The Bode plots in Fig. 6 also include the estimated transfer function for the motor.

An essential parameter in control system design is the time-delay, which represents the time difference between a commanded signal and the sensor measurement. To estimate this time-delay in TU-Flex's control system, a straightforward two-step experimental procedure was implemented: a pre-programmed maneuver within the FCS computer was utilized to generate a step or sweep command signal sent to a specific control surface; the acquired data from the experiment was then post-processed. This involved analyzing the input (actuator command) and the corresponding output (position measured by the servo) to determine the time-delay between the two signals. Following this procedure, the estimated time-delay in the TU-Flex control system was approximately 20 milliseconds, as demonstrated for the internal aileron in Fig. 7. This delay was also observed in all other actuators.

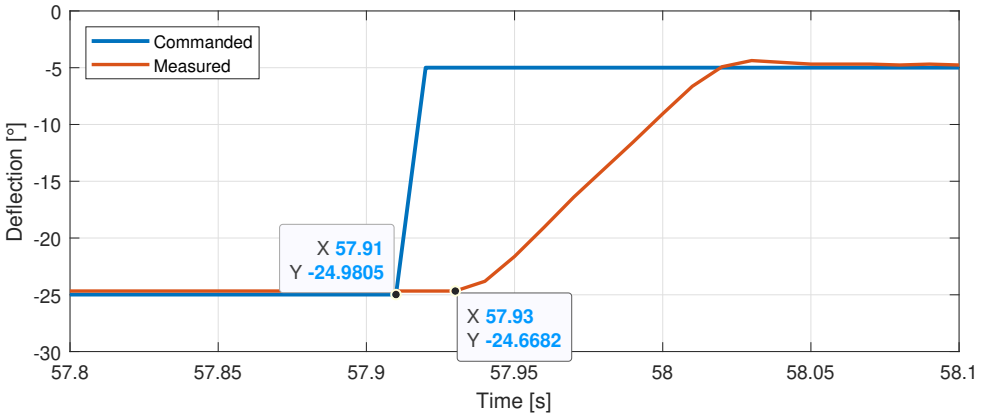


Figure 7: A step signal with a 20-degree amplitude, starting at -25 degrees, applied to the internal aileron.

## 3 CONTROL DESIGN

A SAS was designed to enhance the handling qualities of the TU-Flex and alleviate loads on its wings. The SAS design considered a linearized model of the TU-Flex in straight and level flight at 30 m/s. The model incorporated atmospheric density values from the International Standard Atmosphere (ISA) at a cruise altitude of 100 m. Additionally, the design considered actuator dynamics and a third-order Padé approximation of the estimated time-delay, as discussed in the previous section. The wind tunnel test campaign focused solely on the wing, and therefore, data for rudder and elevator dynamics was not yet available. To address this gap, the dynamic characteristics of the most similar control surfaces on the wing, the flap and internal aileron, were adopted as surrogates for the elevator and rudder, respectively. The impact of including these elements will be analyzed in section 3.2.

The following design requirements were considered for the SAS design:

- Spiral stability: Ensure the spiral mode stability;
- Dutch roll: Achieve closed-loop Dutch roll damping exceeding 0.20, natural frequency greater than 0.16 Hz, following the most stringent guidelines from MIL-F-8785C Dutch-roll-mode specifications [33];

- Phugoid: Achieve closed-loop Phugoid mode damping exceeding 0.04, adhering to the most stringent MIL-F-8785C Phugoid-mode specifications [33];
- Short-period: Achieve closed-loop Short-Period mode damping exceeding 0.35, following the most stringent MIL-F-8785C Short-Period-mode specifications [33];
- Frequency response margins: Maintain a phase margin of at least 45° and a gain margin of 6 dB across the entire flight envelope, as recommended by common practices in flight control design [33, 34];
- Aeroelastic modes: Enforce a minimum damping ratio of 20% and a natural frequency higher than 4.50 Hz for the first and second aeroelastic modes.

The primary objective of the aeroelastic modes requirements is to decouple the structural dynamics (aeroelastic modes) from the rigid-body dynamics of the TU-Flex. This minimizes the influence of wing flexibility on the aircraft's overall flight response, improving handling characteristics.

The selection of a minimum damping ratio (20%) and natural frequency (4.50 Hz) for the first and second aeroelastic modes serve specific purposes: the 20% minimum damping aims to enhance the controllability of the aircraft by mitigating the impact of inherent structural flexibility, particularly in lightly damped modes; the 4.50 Hz natural frequency requirement ensures the aeroelastic modes resonate at least 100% higher than the short-period mode frequency. This separation helps to minimize interaction between the two sets of dynamics, promoting decoupling. Additionally, increasing the damping of the elastic modes contributes to reducing the vibratory loads experienced by the wings during flight.

All aircraft actuators can be independently commanded, but to simplify the input while maintaining control over different flight dynamics, the SAS employs a combination of symmetric and antisymmetric actuation on specific control surfaces. This selection aligns with the characteristics of the mode being controlled:

- Spiral Mode: The external ailerons deflect antisymmetrically to counteract undesired rolling tendencies;
- Phugoid Mode: Symmetrical deflection of both engine thrusts regulates the aircraft's climb and descent;
- Short-Period Mode: The elevators operate symmetrically to manage pitch variations;
- Dutch Roll Mode: The rudder (a single control surface) provides directional control to counter Dutch roll oscillations;
- First Bending Mode: The symmetric nature of this mode is addressed using symmetrical deflection of the mid ailerons;
- Second Bending Mode: To counter the antisymmetric nature of this mode, the flaps are employed with antisymmetrical deflection.

Then the input vector can be rewritten as:

$$\mathbf{u} = \begin{bmatrix} \delta_{ae} \\ \delta_{Th} \\ \delta_{et} \\ \delta_{rd} \\ \delta_{am} \\ \delta_{fp} \end{bmatrix} = \begin{bmatrix} \delta_{ae,r} - \delta_{ae,l} \\ \delta_T \\ \delta_e \\ \delta_r \\ \delta_{am,r} + \delta_{am,l} \\ \delta_{f,r} - \delta_{f,l} \end{bmatrix} \tag{4}$$

that is, $\mathbf{u} \in R^{6\times1}$. This choice of input vector implies the following restructuring of Eq. (2):

$$\mathbf{B}_\delta = \left[\mathbf{B_7} - \mathbf{B_8} \vdots \mathbf{B_{12}} \vdots \mathbf{B_2} \vdots \mathbf{B_{11}} \vdots \mathbf{B_5} + \mathbf{B_6} \vdots \mathbf{B_9} + \mathbf{B_{10}}\right] \tag{5}$$

where $\mathbf{B_j}$ represents the $j$-th column of the matrix $\mathbf{B}$, with $\mathbf{B}_\delta \in R^{n\times6}$. Therefore, the linear model employed in the SAS design is given by:

$$\begin{aligned} \dot{\mathbf{x}} &= \mathbf{A}\mathbf{x} + \mathbf{B}_\delta\mathbf{u} \\ \mathbf{y} &= \mathbf{C}\mathbf{x} \end{aligned} \tag{6}$$

The total control input is given by:

$$\mathbf{u} = \mathbf{R} + \mathbf{u_{sas}} \tag{7}$$

where $\mathbf{R}$ corresponds to pilot inputs and $\mathbf{u_{sas}}$ to the SAS control law, given by:

$$\begin{aligned} \mathbf{u_{sas}} &= -\mathbf{K}\mathbf{y_{sas}} = -\mathbf{K}\mathbf{C_{sas}}\left(\mathbf{C}\mathbf{x}\right) \\ &= -\mathbf{K}\mathbf{C_{sas}}\mathbf{C}\mathbf{x} \\ &= -\underbrace{diag(K_{sl}, K_{ph}, K_{sp}, K_{dr}, K_{\eta1}, K_{\eta2})}_{\mathbf{K}} \underbrace{\begin{bmatrix} \phi \\ V \\ q \\ r \\ \eta_1 \\ \eta_2 \end{bmatrix}}_{\mathbf{y_{sas}}} \end{aligned} \tag{8}$$

with $\mathbf{C_{sas}}$ being a selection matrix of the outputs of interest ($\mathbf{y_{sas}}$). In the context of $\mathbf{K}$ gains, the subscript notation denotes the specific mode targeted for attenuation. Here, $sl$ signifies the gain attenuating the spiral mode, $ph$ for the phugoid mode, $sp$ for the short-period mode, $dr$ for the Dutch roll mode, $\eta_1$ for the first elastic mode, and $\eta_2$ for the second elastic mode. The choice of $\eta$ feedback hinges on aircraft flexibility. Very flexible aircraft require feedback utilizing both the modal amplitudes ($\eta$) and their time derivatives ($\dot{\eta}$) to attain the desired control performance. This comprehensive approach ensures effective control of the elastic modes. Conversely, less flexible aircraft may only necessitate feedback on the time derivative ($\dot{\eta}$), particularly for the second elastic mode ($\eta_2$). This simplification is often sufficient due to the inherently lower modal activity in these aircraft and the higher frequency of the mode.

Table 3: Open- and closed-loop damping ratio and natural frequency values, considering the flexible aircraft model, with and without the servo dynamics and time-delay.

| | Open Loop | | CL Without Dyn. | | CL With Dyn. | |
|---|---|---|---|---|---|---|
| | $\omega_n$ [Hz] | $\zeta$ | $\omega_n$ [Hz] | $\zeta$ | $\omega_n$ [Hz] | $\zeta$ |
| Spiral | 0,007 | 1,00 | 0,543 | -1,00 | 0,498 | -1,00 |
| Phugoid | 0,066 | -0,05 | 0,056 | -0,74 | 0,058 | -0,75 |
| Short-Period | 1,563 | -0,37 | 1,652 | -0,64 | 1,917 | -0,71 |
| Dutch Roll | 0,654 | -0,11 | 0,754 | -0,73 | 0,900 | -0,80 |
| $\eta_1$ | 5,439 | -0,39 | 5,939 | -0,85 | 5,049 | -0,80 |
| $\eta_2$ | 8,076 | -0,11 | 8.581 | -0,21 | 8,124 | -0,20 |

Table 4: Open- and closed-loop damping ratio and natural frequency values, considering the very flexible aircraft model, with and without the servo dynamics and time-delay.

| | Open Loop | | CL Without Dyn. | | CL With Dyn. | |
|---|---|---|---|---|---|---|
| | $\omega_n$ [Hz] | $\zeta$ | $\omega_n$ [Hz] | $\zeta$ | $\omega_n$ [Hz] | $\zeta$ |
| Spiral | 0,007 | 1,00 | 0,428 | -1,00 | 0,329 | -1,00 |
| Phugoid | 0,063 | -0,06 | 0,056 | -0,53 | 0,056 | -0,78 |
| Short-Period | 1,733 | -0,30 | 1,238 | -0,91 | 1,549 | -0,82 |
| Dutch Roll | 0,644 | -0,13 | 0,711 | -0,77 | 0,658 | -0,81 |
| $\eta_1$ | 2.339 | -0,40 | 4.837 | -0,78 | 4.563 | -0,52 |
| $\eta_2$ | 4.400 | -0,12 | 5.228 | -0,21 | 4.537 | -0,20 |

The gain matrix $\mathbf{K}$ is calculated using the Root Locus method, one mode at a time. The sequence starts with the improvement of rigid-body modes, on the following sequence: spiral, phugoid, short-period, and Dutch roll. Once these are addressed, the first and then the second elastic modes are attenuated. The feedback varies for each model used due to their differing dynamics, requiring specific adjustments to achieve the goals. An example of one of the Root Locus plots is shown in Fig. 8, illustrating the feedback of the first elastic mode time derivative of the modal amplitude to the symmetric middle ailerons input, for the very flexible aircraft. The root locus analysis further reveals the coupling between the first elastic mode and the short-period mode.

Table 3 summarizes the damping ratios and natural frequencies of the open-loop and closed-loop modes for the flexible aircraft. The control law successfully achieved the design requirements. Notably, for the rigid-body modes, the achieved damping exceeded the requirements, with most exceeding 0.7. In the absence of established reference values for remotely piloted experimental aircraft, this improvement in damping is expected to enhance flight handling qualities based on operational experience [35]. Table 4 presents similar results for the very flexible aircraft, where increasing the frequency of the elastic modes becomes a critical objective.

Fig. 9 presents the Multiple-Input-Multiple-Output (MIMO) stability margins of the closed-

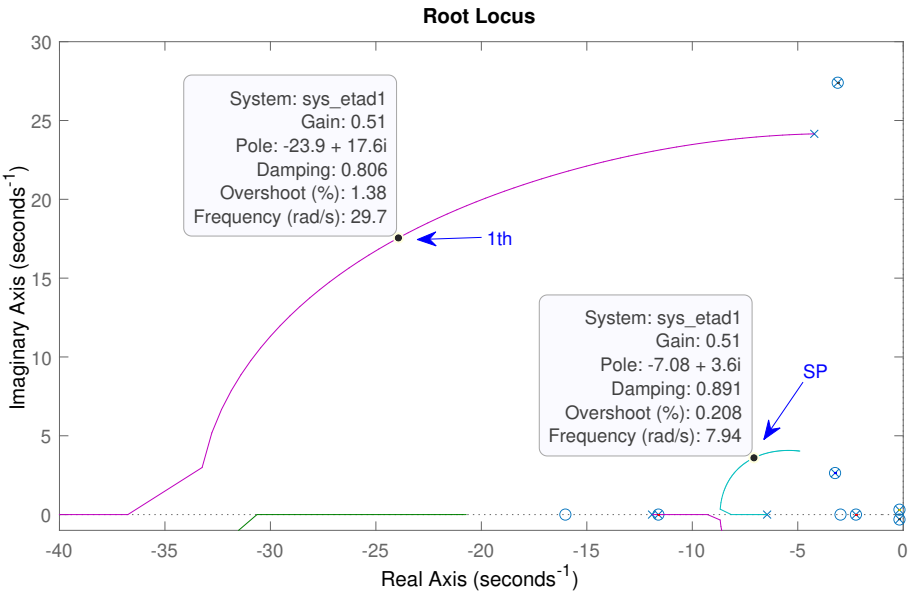


Figure 8: Feedback of the first elastic mode time derivative of the modal amplitude to the symmetric middle ailerons input, for the very flexible aircraft.

Table 5: Disk-based stability margins of feedback loops, considering the very flexible aircraft model, with and without the servo dynamics and time-delay.

| | Worst Single Loop Disk Margin | | | Multiloop Output Disk Margin | | |
|---|---|---|---|---|---|---|
| | GM [Db] | PM [deg] | Fr. [Hz] | GM [Db] | PM [deg] | Fr. [Hz] |
| Flex. Without Dyn. | 15.92 | 71.83 | 6.43 | 11.85 | 61.33 | 0.26 |
| Flex. With Dyn. | 10.20 | 63.43 | 6.88 | 8.22 | 47.56 | 8.21 |
| Very Flex. Without Dyn. | 16.26 | 80.16 | 8.05 | 9.18 | 51.66 | 20.52 |
| Very Flex. With Dyn. | 9.98 | 70.29 | 7.14 | 7.21 | 42.88 | 24.97 |

loop system, calculated using the method outlined in Ref. [36] for both the flexible and very flexible aircraft designs. The margins presented here were derived from two sets of models: those that neglect the dynamics of the actuators and those that incorporate them. From the information displayed, it is possible to see that the inclusion of actuator dynamics leads to a slight decrease in stability margins. It is important to note that the analysis provides a more conservative estimate [35], once this approach considers independent, concurrent variations in both system inputs and outputs within the feedback loop. Although the margins in Fig. 9 may not meet the initial requirements, Table 5 demonstrates that multiloop and loop-at-a-time stability margins satisfy the design criteria.

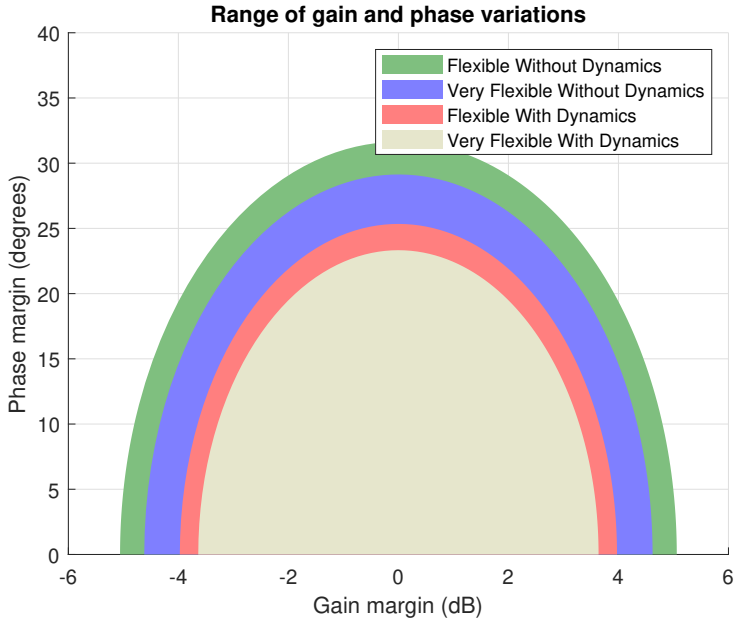


Figure 9: Disk-based stability margins for both aircraft models and servo dynamics plus time-delay.

### 3.1 Interaction of Rigid-Body Control with Flexible Modes

A study on the impact of the rigid-body controller on the elastic modes was conducted as part of the design process. To investigate this, a controller was designed for a rigid-body model, neglecting all elastic effects. This controller was then applied to the full-order model, which includes both rigid-body and flexible dynamics.

Fig. 10 demonstrates that the design successfully meets the flight handling quality requirements. Furthermore, the impact on the flexible modes remains minimal for both the flexible and very flexible aircraft configurations. For the flexible model, the interaction with the elastic modes is negligible. The very flexible model exhibits a slightly greater influence on the first and second elastic modes. However, the impact on the first mode, for example, is a minor decrease in

damping (from 0.39 to 0.36) and frequency (0.07 Hz).

The chosen design approach, along with the selected inputs and outputs, resulted in minimal coupling effects on the attenuation of the rigid-body modes.

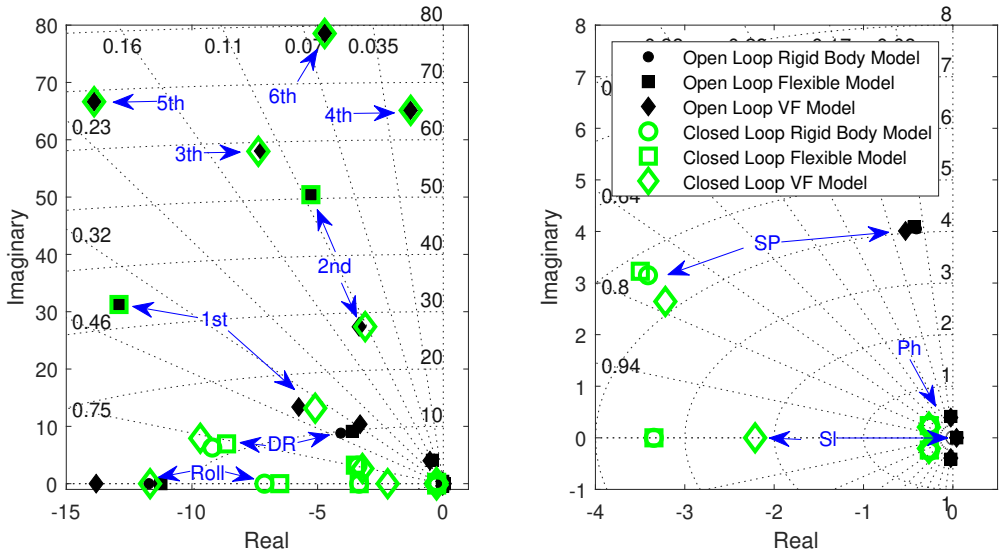


Figure 10: Pole map for rigid body only, flexible and very flexible aircraft. In black are the open-loop poles and in green the closed-loop ones.

### 3.2 Controller Design Considerations: Actuator Dynamics and Time-Delays

Another crucial aspect demanding careful consideration during controller design is the accurate identification and inclusion of actuator dynamics and time-delays [15]. To assess their impact on control performance for both flexible and very flexible aircraft, an analysis similar to the previous section was conducted. Here, the controller was initially designed neglecting the aforementioned dynamics. Subsequently, the obtained gains were applied to a model that incorporates these actuator dynamics and time-delays.

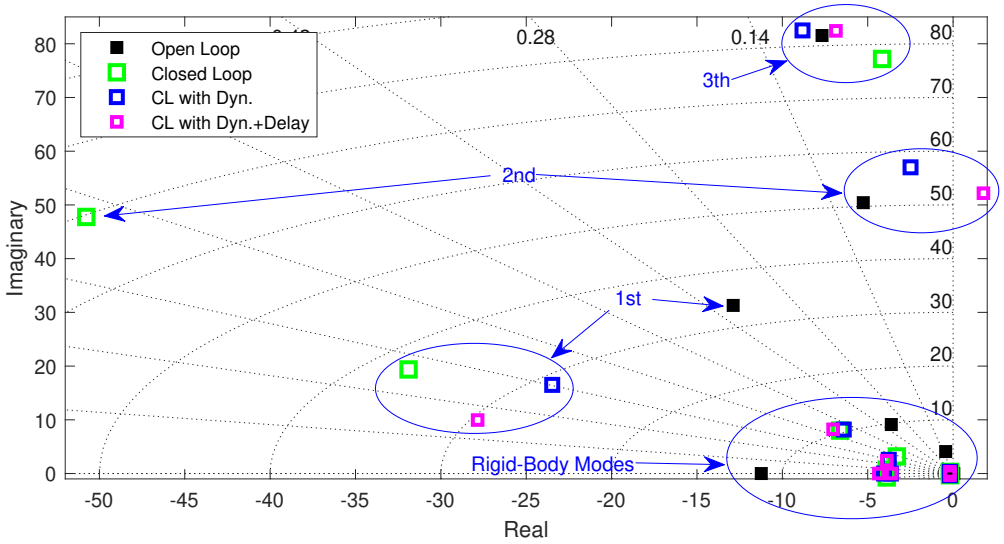


Figure 11: Pole map for open-loop, closed-loop without additional dynamics, closed-loop with actuator dynamics only, and closed-loop with both actuator dynamics and time-delay, for the flexible aircraft model. Lag states and actuator dynamics poles were omitted for better visualization.

In this section, the controller design from the previous section is revisited, with results shown in Table 3. However, this time, the gain is adjusted to target a higher damping ratio (greater than 0.6) in the second elastic mode. This increased damping is expected to significantly reduce the loads experienced by the system. It is important to acknowledge that the controller design excluded the system dynamics. The actuator dynamics and time-delay were added later for evaluation.

Fig. 11 presents the pole map for various configurations of the flexible model: open-loop, closed-loop without additional dynamics, closed-loop with actuator dynamics only, and closed-loop with both actuator dynamics and time-delay. The impact on the rigid-body modes is significant but appears considerably reduced compared to the lower-frequency elastic modes. These elastic modes are heavily influenced by the control actuator and time-delay dynamics. Notably, the second elastic mode experiences a significant decrease in damping when servo dynamics are included. With the additional time-delay, the system becomes unstable. It is important to note that the controller exhibits good gain and phase stability margins, as shown in Table 5.

This behavior can be attributed to the phase shift introduced by the dynamics. At the frequency of the second mode (around 10 Hz), the flap introduces a phase lag of 85 degrees, and the time-delay adds another 75 degrees. This combined phase shift of 160 degrees control signal close to 180 degrees out of phase, essentially causing it to act in opposition to the desired direction.

Similar behavior is observed on the very flexible aircraft, especially for the second elastic mode. A combined phase shift of approximately 120 degrees around 5 Hz also leads to out-of-phase actuation and ultimately, instability. Interestingly, [37] reported a similar phenomenon during the SAS design for the ITA X-HALE, highlighting the need for extra caution with hardware system dynamics in control design for flexible aircraft.

### 3.3 Simulation Results

Linear simulations were conducted to evaluate the proposed controller's effectiveness in attenuating both load and rigid-body motions. Since gust disturbances were not yet incorporated into the models, a symmetric doublet input was applied to the external ailerons for both open-loop and closed-loop systems to assess load reduction. To ensure a fair comparison, the control loop was only activated after the doublet input was concluded.

Fig. 12 presents the rigid-body parameters, highlighting the significant impact on the longitudinal modes due to the symmetric input. The closed-loop response in the figure demonstrates the effectiveness of the proposed controller in attenuating rigid-body motion, both longitudinal and lateral-directional. While the focus of Fig. 12 was on rigid-body parameters, Fig. 13 delves into the structural effects, showing the vertical load at the wing root and the wing tip displacement. By analyzing the first peak after the doublet concludes, we can assess the load reduction achieved by the controller. This analysis reveals a reduction of 40% in load and 42% in wing tip displacement.

Finally, Fig. 14 presents the actuation signals. As expected, the control loop is not activated until after the doublet maneuver concludes. Importantly, all control surface deflections remain within feasible limits (not exceeding 25 degrees for this aircraft). This ensures that the controller achieves its desired effects without exceeding actuator limitations.

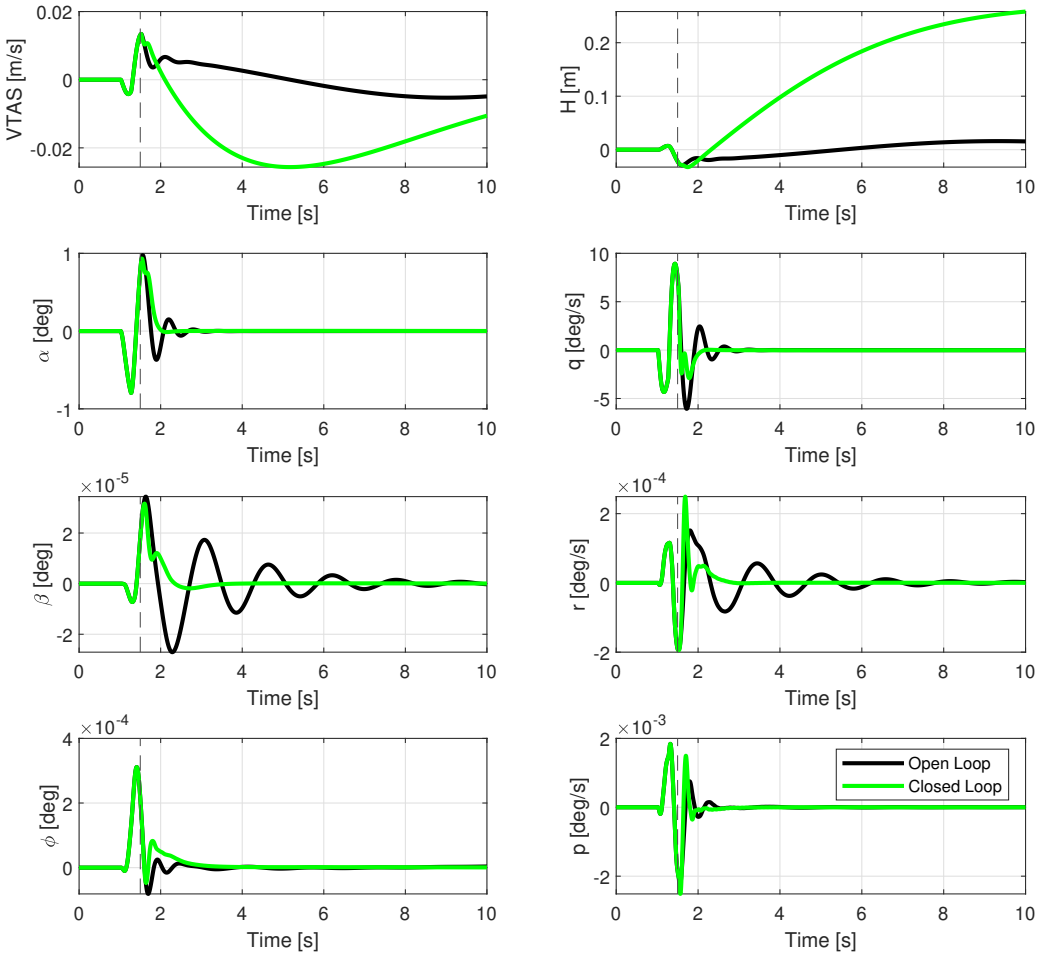


Figure 12: Rigid body outputs for a velocity of 30.0 m/s, subjected to external ailerons symmetric doublet.

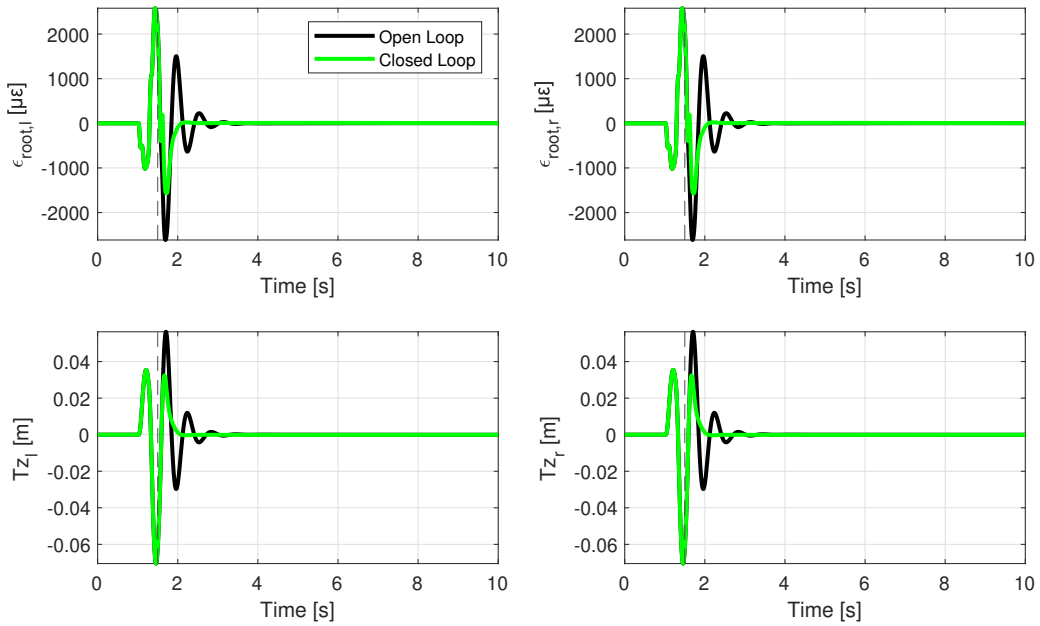


Figure 13: Structural outputs for a velocity of 30.0 m/s, subjected to external ailerons symmetric doublet.

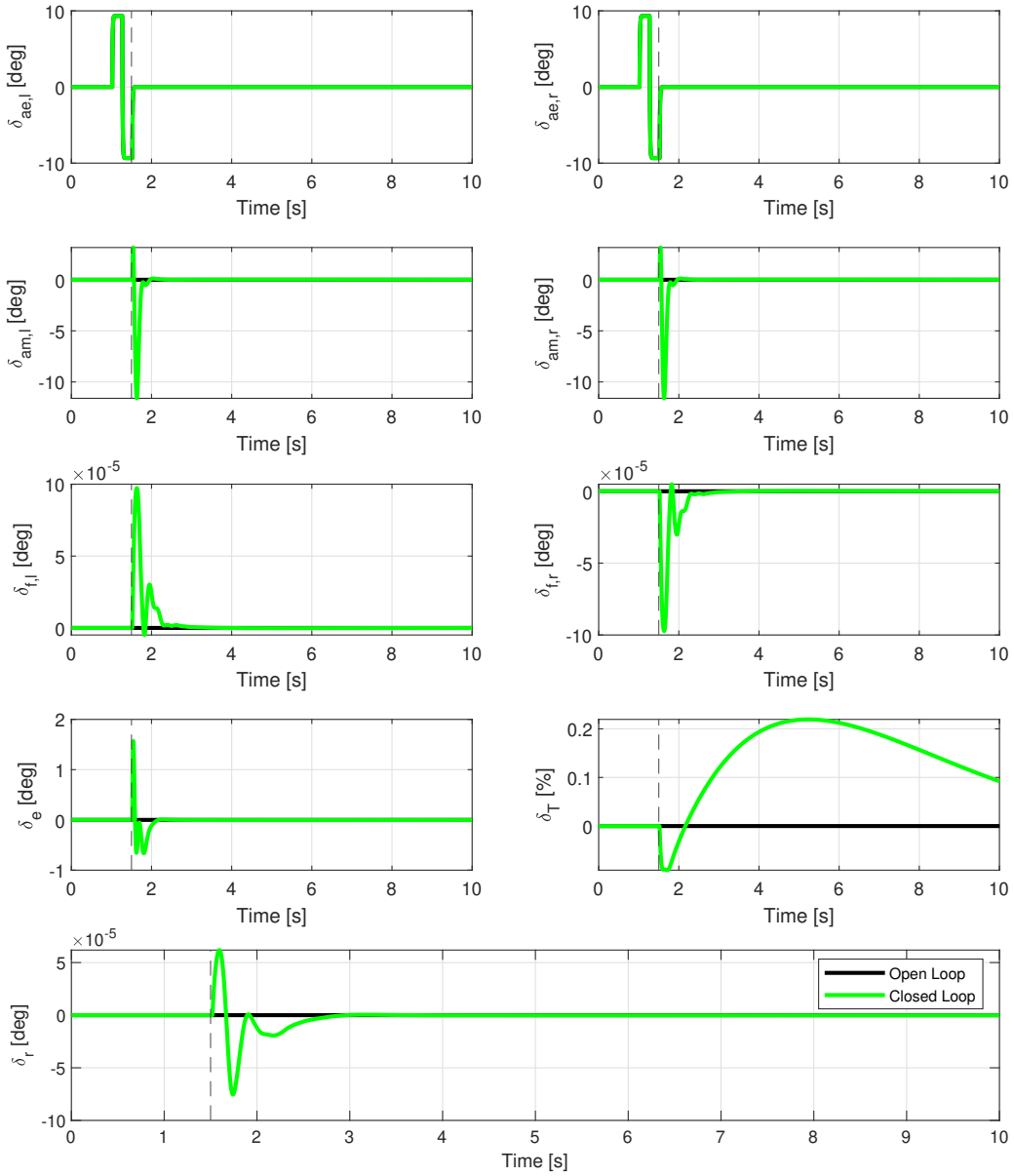


Figure 14: Actuator inputs for a velocity of 30.0 m/s, subjected to external ailerons symmetric doublet.

## 4 CONCLUSIONS

This study demonstrates the success of the designed control law in fulfilling the design objectives for highly flexible aircraft, as evidenced by the combined analysis and simulations. The achieved damping ratios for the rigid-body modes surpass the stipulated requirements, with most exceeding 0.7. This outcome signifies a substantial improvement in flight performance. The control law design methodology, incorporating actuator dynamics and time delays, effectively mitigated the coupling effects between control actions and rigid-body mode attenuation, while successfully addressing the impact on elastic modes.

Building upon the findings from the analysis, the simulations further underscored the potential for enhanced flight handling qualities and system stability through the application of the proposed controller. This observation strengthens the case for the practical implementation of this control strategy in very flexible aircraft.

This study highlights the critical role of incorporating actuator dynamics and time delays into

the control design process for very flexible aircraft. The observed significant impact on elastic modes and system stability emphasizes this necessity. These findings emphasize the importance of accounting for hardware system dynamics within the control design framework to guarantee safe and stable flight operations for flexible and very flexible aircraft.

Overall, the results indicate a successful controller design that meets the design requirements and demonstrates the potential for improved flight handling qualities and system stability for flexible and very flexible aircraft configurations.

## 5 ACKNOWLEDGEMENTS

This study was financed in part by the German Federal Ministry for Economic Affairs and Climate Action (BMWK) due to a resolution of the German Federal Parliament within the scope of the LuFo VI-2 project FlexFuture (Grant number 20E2120A).

## 6 REFERENCES

[1] Palacios, R. and Cesnik, C. E. (2023). *Dynamics of Flexible Aircraft*. Cambridge University Press.

[2] Schmidt, D. K. (2012). *Modern Flight Dynamics*. New York: McGraw-Hill, 1 st ed. ISBN: 978-0-07-339811-2.

[3] Idan, M., Karpel, M., and Moulin, B. (1999). Aeroservoelastic interaction between aircraft structural and control design schemes. *Journal of Guidance, Control, and Dynamics*, 22(4), 513–519. doi:10.2514/2.4427.

[4] Wang, Y., Wynn, A., and Palacios, R. (2016). Nonlinear modal aeroservoelastic analysis framework for flexible aircraft. *AIAA Journal*, 54(10), 3075–3090. doi:10.2514/1.J054537.

[5] Tian, W., Gu, Y., Liu, H., et al. (2021). Nonlinear aeroservoelastic analysis of a supersonic aircraft with control fin free-play by component mode synthesis technique. *Journal of Sound and Vibration*, 493, 115835. ISSN 0022-460X. doi:https://doi.org/10.1016/j.jsv.2020.115835.

[6] Livne, E. (2018). Aircraft active flutter suppression: State of the art and technology maturation needs. *Journal of Aircraft*, 55(1), 410–452. doi:10.2514/1.C034442.

[7] Burnett, E. L., Beranek, J. A., Holm-Hansen, B. T., et al. (2016). Design and flight test of active flutter suppression on the X-56A multi-utility technology test-bed aircraft. *Aeronautical Journal*, 120(1228), 893–909. ISSN 00019240. doi:10.1017/aer.2016.41.

[8] Luspay, T., Ossmann, D., Wuestenhagen, M., et al. *Flight control design for a highly flexible flutter demonstrator*. doi:10.2514/6.2019-1817.

[9] Roessler, C., Stahl, P., Sendner, F., et al. *Aircraft Design and Testing of FLEXOP Unmanned Flying Demonstrator to Test Load Alleviation and Flutter Suppression of High Aspect Ratio Flexible Wings*. doi:10.2514/6.2019-1813.

[10] Waitman, S. and Marcos, A. (2019). Active flutter suppression: non-structured and structured h design *∗this project has received funding from the european union's horizon 2020 research and innovation programme under grant agreement no 636307. *IFAC-PapersOnLine*, 52(12), 146–151. ISSN 2405-8963. doi:https://doi.org/10.1016/j.ifacol.2019.11.184. 21st IFAC Symposium on Automatic Control in Aerospace ACA 2019.

[11] Schmidt, D. K. (2016). Stability augmentation and active flutter suppression of a flexible flying-wing drone. *Journal of Guidance, Control, and Dynamics*, 39(3), 409–422. doi: 10.2514/1.G001484.

[12] Schmidt, D. K., Danowsky, B. P., Kotikalpudi, A., et al. (2020). Modeling, design, and flight testing of three flutter controllers for a flying-wing drone. *Journal of Aircraft*, 57(4), 615–634. doi:10.2514/1.C035720.

[13] González, P., Stavorinus, G., Silvestre, F. J., et al. (2023). Tu-flex: A very-flexible flying demonstrator with a generic transport aircraft configuration. In *AIAA SCITECH 2023 Forum*. doi:10.2514/6.2023-1312.

[14] Silvestre, F. J., Neto, A. B. G. a., Bertolin, R. M., et al. (2017). Aircraft control based on flexible aircraft dynamics. *Journal of Aircraft*, 54(1), 262–271. doi:10.2514/1.C033834.

[15] Sereni, B., Galvão, R. K. H., Assunão, E., et al. (2023). An output-feedback design approach for robust stabilization of linear systems with uncertain time-delayed dynamics in sensors and actuators. *IEEE Access*, 11, 20769–20785. doi:10.1109/ACCESS.2023.3249482.

[16] González, P., Shahi, H., Meddaikar, Y., et al. (2022). Flexible-wing design process for tu-flex demonstrator. In *International Forum on Aeroelasticity and Structural Dynamics - IFASD*. Madrid: Spain.

[17] González, P., Stavorinus, G., Shahi, H., et al. (2022). A preliminary structural design of a flexible flying demonstrator. In *ICAS 2022 - 33rd Congress of the International Council of the Aeronautical Sciences*. Stockholm: Sweden.

[18] Jordan, T., Foster, J., Bailey, R., et al. *AirSTAR: A UAV Platform for Flight Dynamics and Control System Testing*. doi:10.2514/6.2006-3307.

[19] Cunningham, K., Foster, J., Murch, A., et al. *Practical Application of a Subscale Transport Aircraft for Flight Research in Control Upset and Failure Conditions*. doi:10.2514/6.2008-6200.

[20] Schmollgruber, P., Gobert, J.-L., Gall, P.-E., et al. (2010). An innovative evaluation platform for new aircraft concepts. *The Aeronautical Journal*, 114(1157), 451–456. doi: 10.1017/S0001924000003936.

[21] Kuehme, D., Alley, N. R., Phillips, C., et al. *Flight Test Evaluation and System Identification of the Area-I Prototype-Technology-Evaluation Research Aircraft (PTERA)*. doi: 10.2514/6.2014-2577.

[22] Wilson, T., Kirk, J., Hobday, J., et al. (2019). Small scale flying demonstration of semi aeroelastic hinged wing tips. In *International Forum on Aeroelasticity and Structural Dynamics - IFASD*. Savannah: USA.

[23] Guimarães Neto, A. B., Barbosa, G. C., Paulino, J. A., et al. (2023). Flexible aircraft simulation validation with flight test data. *AIAA Journal*, 61(1), 285–304. doi:10.2514/1.J060960.

[24] Cesnik, C. E. S., Senatore, P. J., Su, W., et al. (2012). X-hale: A very flexible unmanned aerial vehicle for nonlinear aeroelastic tests. *AIAA journal*, 50(12), 2820–2833.

[25] Schmidt, D. K., Danowsky, B. P., Seiler, P. J., et al. *Flight-Dynamics and Flutter Analysis and Control of an MDAO-Designed Flying-Wing Research Drone*. doi: 10.2514/6.2019-1816.

[26] NASA. Openvsp. `https://openvsp.org/`. Retrieved on: 2024.

[27] Altair hypermesh. `https://altair.com/hypermesh`. Retrieved on: 2024.

[28] Klimmek, T. (2009). Parameterization of topology and geometry for the multidisciplinary optimization of wing structures. In *CEAS 2009 - European Air and Space Conference*.

[29] Klimmek, T. (2014). Parametric set-up of a structural model for fermat configuration aeroelastic and loads analysis. *Journal of Aeroelasticity and Structural Dynamics*, 3(2). doi:10.3293/asdj.2014.27.

[30] Quesada, A. A. G., González, P. J., Barbosa, G. C., et al. (2024). Influence of nonlinear aerodynamic effects on high aspect ratio aircraft model. In *IFASD 2024 - International Forum on Aeroelasticity and Structural Dynamics*. The Hague, Netherlands.

[31] Schröder, B.-O., González, P., and Silvestre, F. (2022). Testing and modelling of a ducted fan motor for uav applications. In *ICAS 2022 - 33rd Congress of the International Council of the Aeronautical Sciences*. Stockholm, Sweden.

[32] Gonzáles, P. J., Quesada, A. A. G., Barbosa, G. C., et al. (2024). Wind tunnel testing and modal validation of tu-flex's high aspect ratio wings. In *21th International Forum on Aeroelasticity and Structural Dynamics, IFASD 2024*. The Hague, Netherlands.

[33] Stevens, B. L., Lewis, F. L., and Johnson, E. N. (2015). *Aircraft control and simulation: dynamics, controls design, and autonomous systems*. John Wiley & Sons, 3 nd ed.

[34] Eugene, L., Kevin, W., and Howe, D. (2013). *Robust and adaptive control with aerospace applications*. London: Springer.

[35] Bertolin, R. M., Guimarães Neto, A. B., Barbosa, G. C., et al. (2021). Design of stability augmentation systems for flexible aircraft using projective control. *Journal of Guidance, Control, and Dynamics*, 44(12), 2244–2262. doi:10.2514/1.G005783.

[36] JAMES D. BLIGHT, R. L. D. and GANGSAAS, D. (1994). Practical control law design for aircraft using multivariable techniques. *International Journal of Control*, 59(1), 93–137. doi:10.1080/00207179408923071.

[37] Barbosa, G. C., Bertolin, R. M., Paulino, J. A., et al. (2022). Design and flight test of a stability augmentation system for a flexible aircraft. *Journal of Guidance, Control, and Dynamics*, 45(9), 1709–1723. doi:10.2514/1.G006271.

## COPYRIGHT STATEMENT